ADVANCED FUNCTIONAL MATERIALS
www.afm-journal.de

Endo/Lysosome-Escapable Delivery Depot for Improving BBB Transcytosis and Neuron Targeted Therapy of Alzheimer's Disease

Lulu Cai, Chuanyao Yang, Wenfeng Jia, Yuwei Liu, Rou Xie, Ting Lei, Zhihang Yang, Xueqin He, Rongsheng Tong, and Huile Gao**

The effective treatment of Alzheimer's disease (AD) is hindered due to the hard blood–brain barrier (BBB) penetration and non-selective distribution of drugs in the brain. Moreover, the complicated pathological mechanism of AD involves various pathway dysfunctions that limit the effectiveness of a single therapeutic drug. Herein, a dendrigraft poly-L-lysines (DGL)-based siRNA and D peptide (Dp) loaded nanoparticle is designed that could target and penetrate through the BBB, enter the brain parenchyma, and further accumulate at the AD lesion. In this system, T7 peptide, which specifically targets transferrin receptors on the BBB, is linked to DGL via acid-cleavable long polyethylene glycol (PEG) to achieve high internalization, quick escape from endo/lysosome, and effective transcytosis. Then, the Tet1, which specifically targets diseased neurons, is modified onto DGL by short PEG. After being exposed, Tet1 could drive the nanoparticles to the AD lesion and release the drugs. As a result, the production of β amyloid plaques (Aβ) is inhibited. Neurotoxicity induced by Aβ plaques and tau proten phosphorylation (p-tau) tangle is also alleviated, and the cognition of AD mice is significantly improved. Overall, this system programmatically targets BBB and neurons, thus, significantly enhances the intracephalic drug accumulation and AD treatment efficacy.

1. Introduction

Alzheimer's disease (AD) is an irreversible and progressive degeneration of the brain that destroys memory, cognition, and other functions, ultimately leading to death from bodily functions lost and complete brain failure.[1] AD affects the quality of life of the elderly seriously and causes economic loss of society. To treat AD, researchers and companies have been developing many candidate compounds, proteins, and even therapeutic genes, which show great promise in vitro. Unfortunately, most of them failed in clinical trials because of the poor drug delivery efficiency and complicated pathological mechanisms involved. Nanoparticle-based drug delivery systems (DDSs) could overcome the shortages of many drugs and provide promising solutions in various diseases, such as cancer and inflammation.[2,3] However, it remains a challenge to develop effective DDSs for the treatment of AD. First, as a homeostatic defense barrier of the brain, the blood–brain barrier (BBB) restricts the entry of almost all the macromolecules and over 98% small molecular drugs.[4] Second, even luckily overcoming the BBB, drugs would be hard to specifically distribute into neurons or AD lesions due to the complicated brain conditions. Finally, the intricate pathological mechanism of AD involves various pathway dysfunctions that require synergistic treatments using multiple drugs.[5,6] Therefore, designing a promising DDSs for AD, which may overcome the above three challenges, has drawn remarkably increased attention in recent years.

To overcome the BBB, many strategies have been developed,[7,8] among which receptor-mediated transcytosis (RMT) combined with the advances of nanotechnology is the most widely used. RMT is based on the specific interaction between ligands on nanoparticles and receptors on endothelial

L. Cai, C. Yang, R. Tong
Personalized Drug Therapy Key Laboratory of Sichuan Province
Department of Pharmacy
Sichuan Provincial People's Hospital
School of Medicine
University of Electronic Science and Technology of China
Chengdu 610072, P. R. China
E-mail: tongrongsheng@med.uestc.edu.cn, tongrs@126.com

The ORCID identification number(s) for the author(s) of this article can be found under https://doi.org/10.1002/adfm.201909999.

DOI: 10.1002/adfm.201909999

C. Yang, W. Jia, Y. Liu, R. Xie, T. Lei, Z. Yang, X. He, H. Gao
Key Laboratory of Drug-Targeting and Drug Delivery System
of the Education Ministry and Sichuan Province
Sichuan Engineering Laboratory for Plant-Sourced Drug and Sichuan
Research Center for Drug Precision Industrial Technology
West China School of Pharmacy
Sichuan University
Chengdu 610041, P. R. China
E-mail: gaohuile@scu.edu.cn
H. Gao
Key Laboratory of Smart Drug Delivery (Fudan University)
Ministry of Education
Shanghai 201203, P. R. China

cells of BBB.[9,10] After being recognized by receptors on the lumen, nanoparticles would be internalized into endo/lysosomes. Thus, many studies focus on finding specific targeting ligands that have high affinity with brain microvessel endothelial cells to enhance the recognition and endocytosis of nanoparticles.[11–13] Nevertheless, ligands with high binding affinity are not easily separated from receptors after recognition, which causes difficulty in escaping lysosomes and restricts the following exocytosis of drugs to brain parenchyma.[14] Hence, it requires the DDSs for AD to not only maintain high BBB selectivity but also separate quickly from membrane receptors after endocytosis.

In our previous study, an acid-responsive glioma targeting delivery system was designed with an improved BBB transcytosis rate due to its ability to escape from the endo/lysosomes.[15] Based on the mentioned strategy, the T7 peptide (HAIYPRH), which has high affinity with the transferrin receptor (TfR) on the BBB, was used as the first targeting ligand.[16,17] T7 was easy to synthesize and not competed by endogenous transferrin with small steric hindrance and great stability.[18] To equip with endosome detachable property, an acid response linker was modified between nanocarriers and T7 via a long bifunctional polyethylene glycol (PEG).[15] After being endocytosed into endo/lysosome, T7 with long PEG will detach from nanoparticles, enabling the nanoparticles separating from TfR to enter brain parenchyma. Besides, it is necessary for nanoparticles to specifically target AD lesions after being transported to the brain parenchyma. To satisfy the requirement, a 12-amino-acid peptide Tet1 was chosen as the second targeting ligand which was modified onto carriers via a short bifunctional PEG. It could specifically bind to the highly expressed sphingomyelin and ganglioside GT1B on neurons to improve the AD targeting of nanoparticles.[19–21]

β amyloid (Aβ) plaques deposition and tau protein phosphorylation (p-tau) neurofibrillary tangles are two of the hallmark neuropathologic indicators of AD.[6,22–24] And both of them promote each other to cause neurotoxicity in the pathogenesis of AD.[25–27] It is reported that β-site amyloid precursor protein (APP) cleaving enzyme 1 (BACE1) is overexpressed in neurons and hydrolyzes the APP to Aβ.[28,29] Thus, small interfering RNA (siRNA) technology has been used to down-regulate the BACE1 expression for reducing the production and deposition of Aβ.[30–34] On the other hand, owing to abnormal phosphorylation, tau protein tends to aggregate into fibers. An all D-amino acid inhibitor (Dp, sequence: D-TLKIVWGKKKC) showed the capacity of ameliorating the neuropathology in AD mice by inhibiting tau phosphorylation and reducing tau fibril formation.[35,36] Therefore, co-delivery BACE1 siRNA and Dp might be promising for AD treatment.

Herein, dendrigraft poly-L-lysines (DGL), a kind of amphiphilic cationic polymer for gene delivery with low toxicity and high gene transfection efficiency,[37,38] was used as a vehicle for BACE1 siRNA and Dp. First, Dp and Tet1 were modified onto DGL with short-chain PEG (MW 1000) (D-DT). Then, T7 peptide was linked with an acid-cleavable long-chain PEG (MW 6000) and modified on the DGL (D-DTCT7). Finally, the BACE1 siRNA was loaded on the D-DTCT7 by static electricity to obtain the AD targeting dual-drug delivery depot (D-DTCT7/siRNA) (**Figure 1**). Acid-uncleavable T7 modified on the D-DT as a negative control (D-DTT7/siRNA). In this study, subcellular localization, lysosome escape, and in vitro BBB transcytosis of nanocarriers were evaluated to demonstrate the acid cleavage ability and superiority of the DDSs. In vitro and in vivo targeting efficiency was determined by cellular uptake, in vivo imaging, and fluorescent immunostaining. Then the therapeutic efficacy was illuminated by behavior test, gene silencing, and immunohistochemical evaluation. This system provides an effective method for improving the transcytosis efficiency of BBB and the targeting of neurons, enhancing the drug accumulation at AD lesions and increasing the binary drug's therapeutic effect.

2. Results

2.1. Preparation and Characterization of D-DTCT7/siRNA

First, Dp and Tet1 were modified with short NHS-PEG-NHS (MW 1000) and demonstrated by mass spectrum (Figure S1A,B, Supporting Information). Acid-sensitive PEG chains (NHS-PEG-DAK-PEG-MAL, PDP) and negative control chains (COOH-PEG-PEG-NHS, PP) were synthesized, respectively and demonstrated by mass spectrum (Figure S1C,D, Supporting Information). Then the preparation of siRNA loaded nanoparticles was optimized by particle size, zeta potential, and siRNA encapsulation capacity (**Figure 2**A–C and Figure S2A–D, Supporting Information). Nanoparticles at N/P ratio of 10 showed relatively small particle size (about 130 nm), slightly positive charge, and good siRNA encapsulation capacity, so the N/P ratio of 10 was used in the following experiments. The particle size and zeta potential of all kinds of nanoparticles (N/P = 10) were measured three times by dynamic light scattering (Table S1, Supporting Information). The siRNA drug-loading capacity at N/P = 10 was about 14.9%. An analogous spherical shape and compacted structure were shown in TEM photographs. D-DTCT7 with poor granulation capability tend to aggregate (Figure 2E), while the D-DTCT7/siRNA was more stable and uniform (Figure 2F).

2.2. Stability, Biocompatibility, and siRNA Release of D-DTCT7/siRNA

An important advantage of DGL-carrying siRNA was that cationic polymers can protect siRNA from degradation by RNase. Agarose gel electrophoresis showed that the siRNA bands disappeared after incubation with RNase (Figure 2G), indicating that the naked siRNA was unstable. However, when combined with DGL, siRNA was difficult to be degraded by RNase and remains in the pore. Besides, to investigate the plasma stability of nanoparticles, the absorption of D-DTCT7/siRNA in 450 nm was detected after incubation with 10% and 50% fetal bovine serum (FBS). Higher absorption was observed in medium with higher concentration of FBS because of the serum protein coating onto nanoparticles, which was consistent with our previous reports.[39,40] During 24 h incubation, the absorption showed no obvious increase (Figure S3,

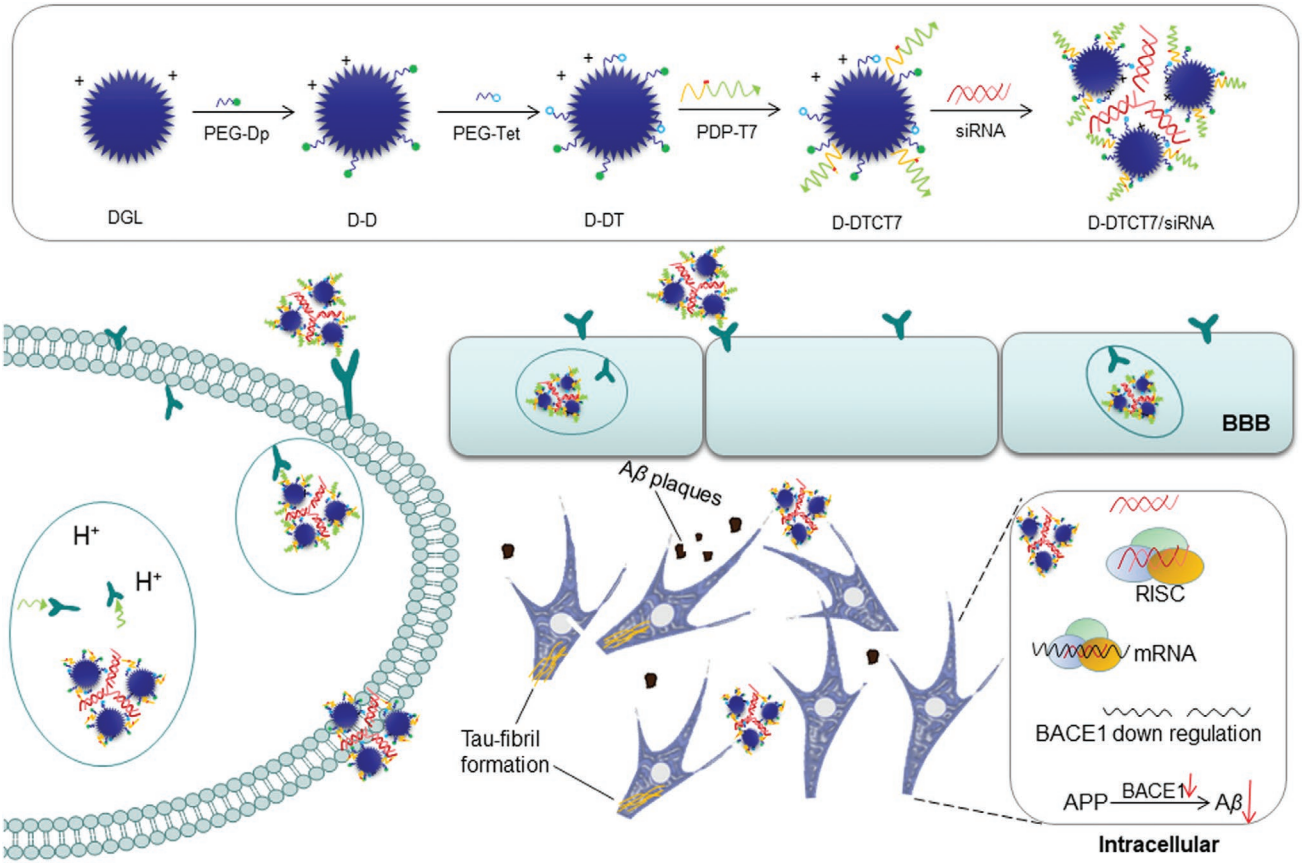

Figure 1. Scheme of the acid-responsive programmed AD-targeted delivery depot for D-DTCT7/siRNA (Aβ, β amyloid; RISC, RNA-induced silencing complex; BACE1, β-site amyloid precursor protein cleaving enzyme 1; APP, Amyloid precursor protein).

Supporting Information). Both results proved that D-DTCT7/siRNA nanoparticles possessed excellent RNase stability and serum stability.

Moreover, strong positive charges of the cationic polymer could destroy the stability of the erythrocyte membrane and lead to aggregation of the erythrocyte.[41] Therefore, hemolysis

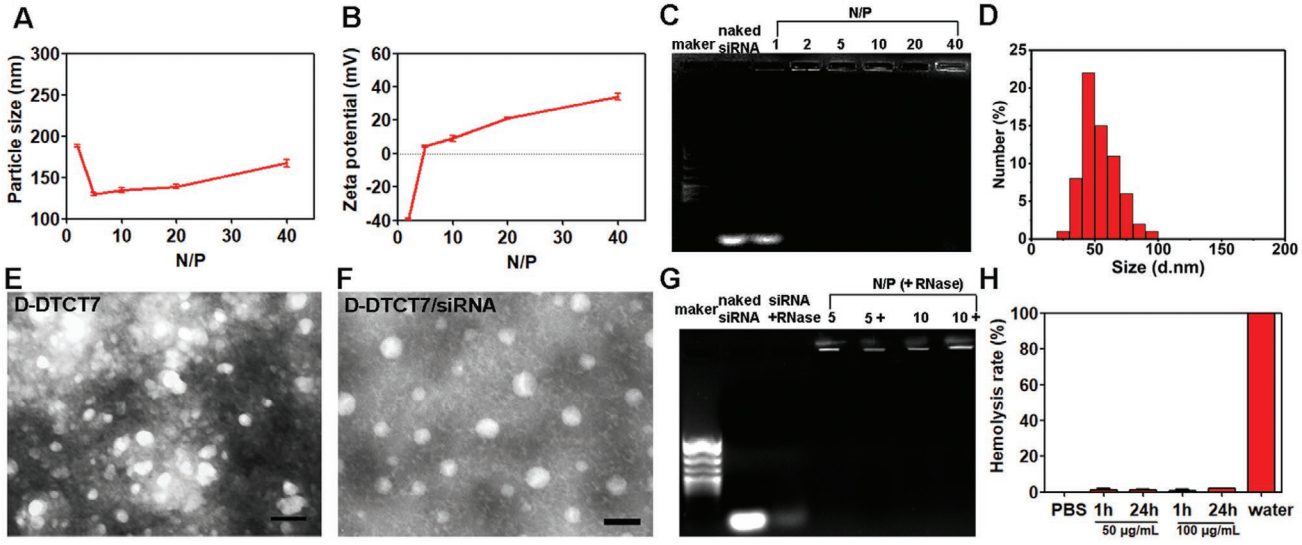

Figure 2. Characterization of the D-DTCT7/siRNA. A,B) The particle size and zeta potential of D-DTCT7/siRNA at different N/P ratios. C) Agarose gel electrophoresis of D-DTCT7/siRNA at different N/P ratios. D) The size distribution of D-DTCT7/siRNA in TEM imaging. E,F) The TEM images of D-DTCT7 and D-DTCT7/siRNA. Scale bars represent 100 nm. G) Agarose gel electrophoresis of D-DTCT7/siRNA after co-incubation with RNase. H) Hemolysis test of D-DTCT7/siRNA in different concentrations and different time.

experiments were conducted to evaluate the biocompatibility of D-DTCT7/siRNA (Figure 2H and Figure S4, Supporting Information). The hemolysis rate of positive control (water) was 100%, while carrier-incubated groups were almost less than 3%. These results showed that the D-DTCT7/siRNA was biocompatible.

siRNA release behavior was important for the efficient treatment of diseases.[32,42] Therefore, the cumulative release rate of siRNA was calculated by measuring the fluorescence intensity of FAM-labeled siRNA to investigate the behavior of siRNA release from nanoparticles (Figure S5, Supporting Information). The 48 h cumulative siRNA release in D-D/siRNA and D-DT7/siRNA was over 80%, while that in D-DTCT7/siRNA was 52.46%. The results suggested siRNA could be sustained release from nanoparticles.

2.3. Intracellular Behavior and Mechanistic Studies

The bEnd.3 is a brain endothelial cell line of murine which has been widely used as a model for simulated brain capillary endothelial cells.[43] The internalization of fluorescein isothiocyanate (FITC) labeled nanoparticles by bEnd.3 cells were observed via confocal imaging after 2 h incubation. The bEnd.3 cellular uptake of D-DTCT7/siRNA was stronger 1.33 and 1.19 times than that of D-D/siRNA and D-DT/siRNA at 4 h, suggesting the T7 could efficiently promote the cellular uptake through RMT pathway because of the over-expression of TfR on bEnd.3 cells.[44] Lysosomal escape ability was evaluated by localization of the nanoparticles and lysosomes in bEnd.3 cells (**Figure 3**A). It showed that the overlay signal of D-DT7/siRNA and D-DTT7/siRNA with endo/lysotracker red were stronger at 2 h, while D-DCT7/siRNA and D-DTCT7/siRNA almost separated from lysosomes. These results supported the acid-sensitive T7 was able to be cleaved from D-DCT7/siRNA and D-DTCT7/siRNA in endo/lysosomes to facilitate intracephalic drug delivery. Then, cellular uptake of different nanoparticles by bEnd.3 cells was also quantified by flow cytometry (Figure 3B). There was no obvious ingestion trend after incubation for 1 h, while the fluorescence intensity of T7-coating nanoparticles was much higher than that of D-D/siRNA after incubation for 2 and 4 h. It was also suggested the T7 could efficiently promote the cellular uptake.

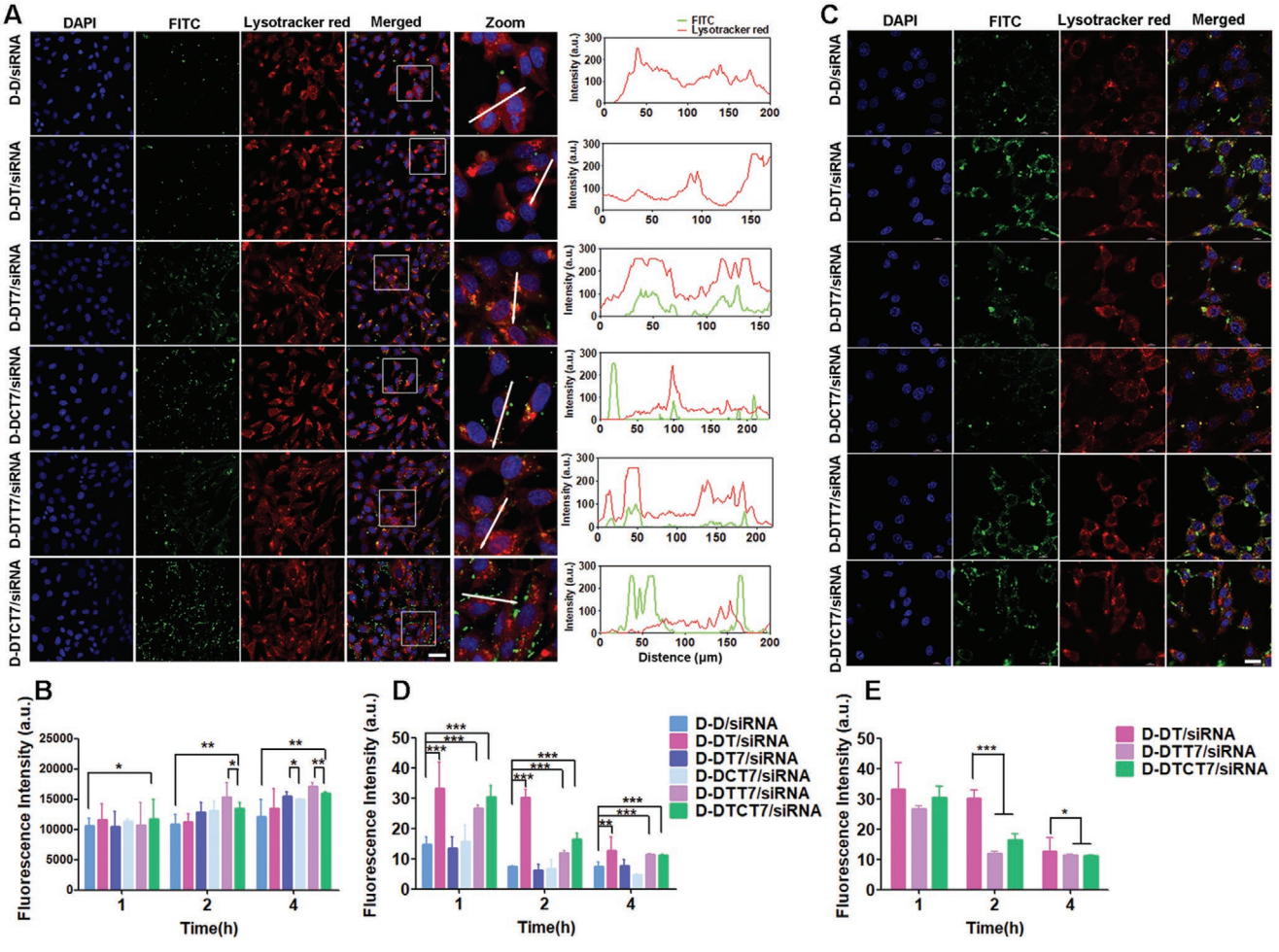

Figure 3. Intracellular behavior studies A) Localization of nanoparticles and lysosomes in bEnd.3 cells after incubation for 2 h. Scale bar represents 50 μm. B) Quantitative uptake of nanoparticles by bEnd.3 cells at different time. C) Confocal fluorescence imaging of nanoparticles uptaken by PC12 cells. Scale bar represents 20 μm. D) Quantitative uptake of nanoparticles by PC12 cells at different time. E) Quantitative uptake of D-DT/siRNA, D-DTT7/siRNA, and D-DTCT7/siRNA by PC12 cells at different time. Data were presented as mean ± SD ($n = 3$).

Stimulated by nerve growth factor, the rat pheochromocytoma cells PC12 can differentiate into neuron-like cells.[45] Hence, PC12 cells were generally used as a model for the study of AD disease.[33] So we studied the PC12 cell uptake of nanoparticles to evaluate the neuron targeting capacity. The confocal imaging showed that D-DT/siRNA had the strongest fluorescence intensity in PC12 cells (Figure 3C). Similarly, the quantitative results showed that D-DT/siRNA, D-DTT7/siRNA, and D-DTCT7/siRNA had relatively stronger fluorescence intensity than that of nanoparticles without Tet1 modification (Figure 3D). The increased endocytosis was due to that Tet1 specifically recognized the receptors on PC12 cells. Importantly, the uptake of D-DTT7/siRNA and D-DTCT7/siRNA was less than that of D-DT/siRNA (Figure 3E), owing to the coverage of long-chain PEG-T7 which might be able to protect the Tet1 in blood circulation.

Also, it was worth noting that the cellular uptake of nanoparticles modified by T7 and Tet1 peptides was stronger than that of nanoparticles without ligand modification (D-D/siRNA). This might be due to the active-targeting mediated by ligand-receptor specific binding. Therefore, we further studied the internalization pathway by adding different uptake inhibitors (Figure S6A,B, Supporting Information). Results showed that several pathways, including caveolae-mediated endocytosis and clathrin vesicles were involved. Then, we used free T7 and Tet1 to block the related receptors on bEnd.3 and PC12 cells for 1 h before cellular uptake (Figure S6C,D, Supporting Information). After adding free T7, the uptake of D-DTT7/siRNA decreased to 60.17% ± 0.039% in bEnd.3 cells. After adding free Tet1, the D-DT/siRNA and D-DTT7/siRNA decreased to inhibit the uptake down to 18.5% ± 0.064% and 27.01% ± 0.045%. These indicated that receptor-mediated endocytosis was one of the major internalization pathways.

2.4. In Vitro Evaluation of Cytotoxicity and BBB Transcytosis

In vitro cytotoxicity experiments were performed in bEnd.3 cells (**Figure 4**A). The DGL had bare toxicity at concentrations lower than 40 μg mL^{-1} which we used in the following experiments.

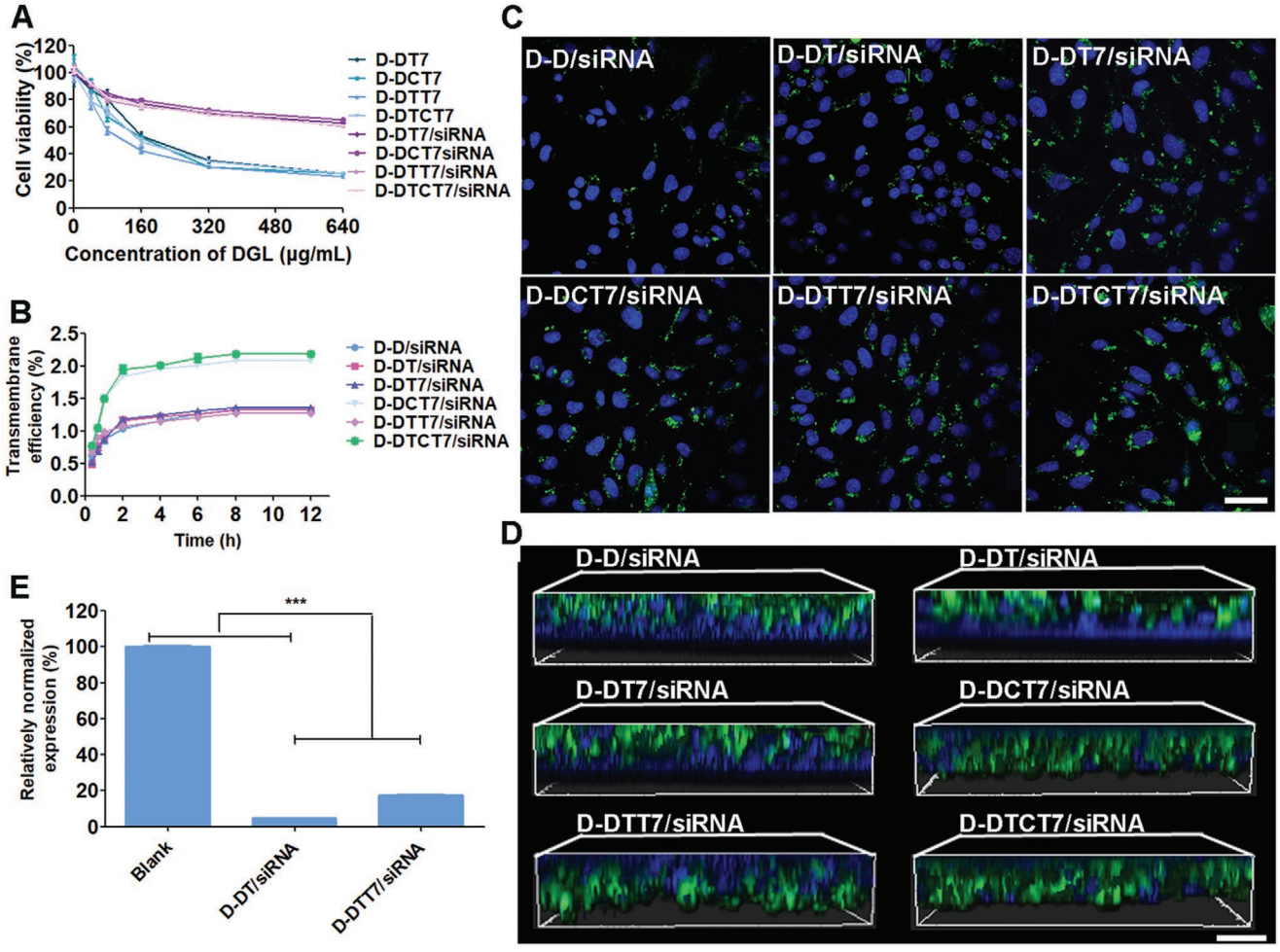

Figure 4. In vitro BBB transcytosis and gene silencing. A) The cell viability incubated with different formulations measured by MTT assay. B) Transcytosis efficiency of different formulations in the BBB model. C) Confocal images showing the internalization of different formulations by PC12 cells in lower chambers of the transwell model after incubation for 4 h. Scale bar represents 50 μm. D) 3D confocal images of bEnd.3 monolayers in the donor chamber of transwell model after the introduction of different formulations for 4 h. Scale bar represents 40 μm. E) Quantitative qRT-PCR analysis showing the expression of BACE1 mRNA in PC12 cells treated with different formulations. Data were presented as mean ± SD ($n = 3$).

To determine the BBB transcytosis capacity of D-DTCT7/siRNA, the bEnd.3 monolayer was established. After cells inoculation, transmembrane resistance of bEnd.3 monolayer was measured every other day by a resistor (Figure S7B, Supporting Information). Until the 12th day, the transmembrane resistance was stable at about 170 Ω, and then the monolayers were incubated with different nanoparticles (FAM-labeled siRNA) to calculate their transmembrane efficiency (Figure 4B). D-DTCT7/siRNA and D-DCT7/siRNA displayed a similar fluorescence intensity, with transcytosis percentages of 2.18% ± 0.05% and 2.08% ± 0.02%, respectively. In contrast, the transcytosis rates of other four groups were all below 1.5%. These results suggested that D-DCT7/siRNA and D-DTCT7/siRNA enhanced the BBB transcytosis compared with non-targeted and non-cleavable groups. We also cultured PC12 cells in the lower chambers of the transwell. After 4 h incubation with the nanoparticles, PC12 cells were removed for fluorescence imaging (Figure 4C). Stronger fluorescence was obtained with D-DTCT7/siRNA than the other groups. The BBB monolayer was also removed and placed on slides. Similar results were obtained in 3D confocal images of BBB monolayer (Figure 4D). The longitudinal (*Z*-axis) displayed that the double-targeted nanoparticles (D-DTT7/siRNA, D-DTCT7/siRNA) and cleavable ligand modified nanoparticles (D-DCT7/siRNA) penetrated deeper than other nanoparticles. These results demonstrated the superiority of double-ligand modification and acid-cleavable linker in designing a DDSs for deep BBB penetration.

2.5. In Vitro Gene Silencing Activity

PC12 cells were treated with D-DT/siRNA and D-DTT7/siRNA for 12 h and the gene silencing effect was analyzed by levels of BACE1 mRNA via quantitative real-time PCR (qRT-PCR) (Figure 4E). The BACE1 mRNA expression of cells treated by D-DT/siRNA was 4.93% ± 0.06% and that by the D-DTCT7/siRNA was 17.58% ± 0.26%, respectively. This result indicated the BACE1 siRNA loaded nanoparticles amplified the BACE1 inhibition efficiency compared with blank groups, indicating that D-DT and D-DTT7 facilitated the siRNA transfection. In vitro, D-DT/siRNA with better gene silencing effect than D-DTT7/siRNA might be because without the T7-PEG shielding, the exposed Tet1 peptide specifically targeted PC12 cells and improved the transfection efficiency.

2.6. In Vivo Distribution

To explore the BBB transcytosis ability and accumulating capacity, the biodistribution of Cy5.5-labeled nanoparticles in AD model mice was monitored by living fluorescent imaging (**Figure 5**A). Nanoparticles linked to T7 showed stronger fluorescence in the brain than that without T7, suggesting that T7 modification could improve brain endothelium uptake and facilitate brain targeting delivery. Over time, the fluorescence in brains increased in groups of D-DCT7/siRNA, D-DTT7/siRNA, and D-DTCT7/siRNA, while not changed obviously in the other two groups. This result demonstrated that dual targets endowed more accumulation of nanoparticles in brains. Moreover, the cleavable T7 modified groups, D-DCT7/siRNA and D-TCT7/siRNA further enhanced the brain delivery compared with the uncleavable groups. Ex vivo imaging of organs (Figure 5B and Figure S8, Supporting Information) showed that D-DTCT7/siRNA nanoparticles had the highest distribution in brains at 48 h, in contrast, nanoparticles in other groups were mainly distributed at the liver and kidney. Simultaneously, the quantification of brain fluorescence (Figure 5C) showed that the brain accumulation of D-DTCT7/siRNA increased to 1.83 times and that of D-DTT7/siRNA increased to 1.64 times compared with D-D/siRNA treatment. Organs and brains were also sliced to observe the accumulation of fluorescence by confocal imaging (Figure S9, Supporting Information and Figure 5D), which were basically consistent with the above results. In summary, the cleavable T7 could effectively improve brain targeting, and Tet1 could further promote the AD targeting drug delivery.

2.7. The Behavioral Test by Morris Water Maze

Morris water maze (MWM) was used to assess the effect of learning acquisition in AD mice treated with different nanoparticles (**Figure 6**A and Figure S10, Supporting Information). In the placed navigation test, the representative swimming paths of mice displayed the aimless circles in PBS and D-D/siRNA treatment groups. By contrast, the mice in D-DTT7/siRNA and D-DTCT7/siRNA groups were purposeful in searching for platforms. The results were also presented statistically by time taken to reach the platform (Figure 6B). Compared with the mice treated with D-DCT7/siRNA (25.7 s ± 25.4 s), D-DTT7/siRNA (18.3 s ± 17.7 s), D-DT7/siRNA (27.9 s ± 23.1 s), D-D/siRNA (41.7 s ± 21.9 s), and PBS (53.4 s ± 13.2 s), the mice treated with D-DTCT7/siRNA took the least time (15.8 s ± 18.3 s) to reach the platform, which was similar to that of healthy mice (15.1 s ± 5.0 s). After training, the spatial probe test was carried out after removing the original platform. The average frequencies for the mice passing through the location of original platform were counted (Figure 6C). The AD mice treated with PBS or D-D/siRNA passed through the platform for less than 1 time, while that of the mice treated by D-DTCT7/siRNA increased to about 3.4 ± 2.4 times. Besides, compared with D-DT7/siRNA and D-DTT7/siRNA groups (2.7 ± 1.8 and 3.0 ± 2.1 times, respectively), the D-DTCT7/siRNA and D-DCT7/siRNA groups passed more times through the platform (3.4 ± 2.4 and 3.4 ± 2.7 times, respectively), suggesting the cleavable T7 modification further amplified the AD treatment efficacy in vivo compared with the non-cleavable T7. These results suggested that the BBB and neuron targeted drug depot significantly improved the intracerebral delivery and ameliorated learning acquisition of AD mice.

2.8. Reduce the Production of Amyloid Plaques In Vivo

Immunofluorescence staining was used to observe the Aβ_{1-42} plaques in the hippocampus and cerebral cortex of transgenic AD mice. There were more and larger plaques in the cortex of AD mice treated with PBS (Figure 6D and Figure S11, Supporting Information), suggesting that the Aβ_{1-42} plaques were

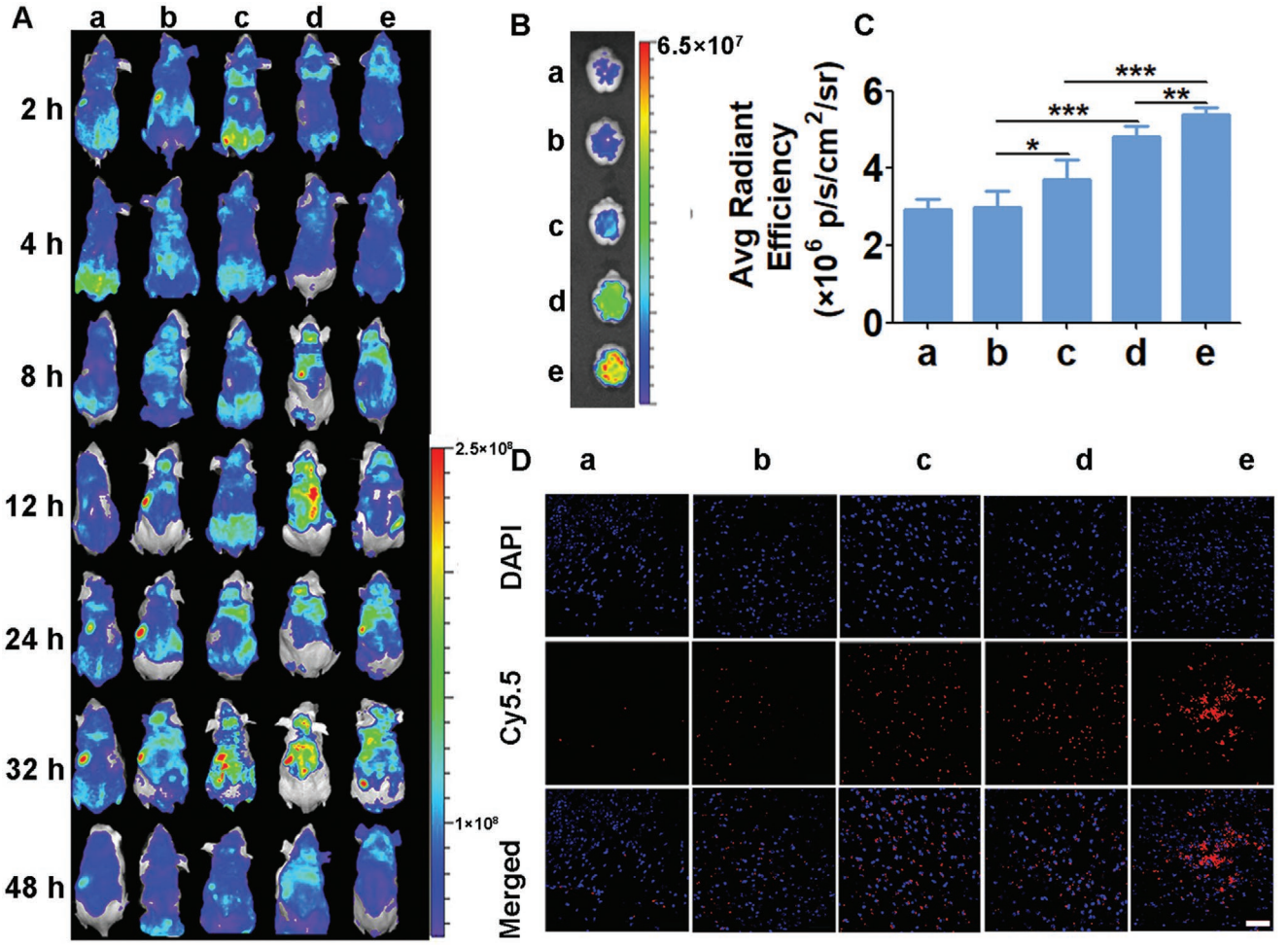

Figure 5. In vivo distribution. A) Living imaging depicting the in vivo distribution of different formulations at different time. B) Ex vivo imaging of brains in different groups after 48 h. C) The quantitative fluorescence intensity of (B). Data were presented as mean ± SD (n = 3). D) Representative confocal fluorescence images of brains showing the accumulation of different nanoparticles: a) D-D/siRNA; b) D-DT7/siRNA; c) D-DCT7/siRNA; d) D-DTT7/siRNA; e) D-DTCT7/siRNA. Scale bar represents 50 µm.

overexpressed in the brains of AD mice. The D-D/siRNA and D-DT7/siRNA nanoparticles treated groups did not exhibit pathologic changes. Excitingly, the Aβ_{1-42} plaques burden was significantly reduced after treatment with D-DTT7/siRNA and D-DTCT7/siRNA nanoparticles. Next, the immunofluorescence staining of Aβ_{1-42} plaques in the hippocampus was consistent with those in the cerebral (Figure S11, Supporting Information). This result indicated that the cleavable T7 and the dual-targeted modification acted together to efficiently deliver siRNA to brain neurons and specifically inhibited the production of toxic isoform Aβ_{1-42} plaques.

2.9. Neuroprotective Effect

The Aβ and tau protein work together to increase Ca^{2+} concentration in synapses and induce neurotoxicity,[26] and Aβ can further promote the phosphorylation and neurotoxicity of tau protein.[25,27] Thus, we used Nissl and H&E staining to evaluate the damage of neurons in hippocampal, which reflected neurotoxicity (**Figure 7**A and Figure S10, Supporting Information). The CA1 area was the most prone to lesions in the hippocampus. So the marked neuronal damage, including neuronal hypocellularity and nuclear shrinkage, were observed in the CA1 hippocampus of the AD mice treated with PBS, or D-D/siRNA. While the above phenomenon was not found in healthy mice, D-DTT7/siRNA and D-DTCT7/siRNA groups, demonstrating that dual-targeted and cleavable T7 formulations attenuated the impairment of neuronal integrity as well as neuron loss. The results of H&E staining in the hippocampus were consistent with Nissl staining (Figure S12, Supporting Information). Additionally, new neurons continued to be generated throughout the adulthood of healthy mammals, and the synaptic changes emerged long before neuronal death in early AD.[46] Therefore, the immunohistochemistry of neuron skeleton protein MAP2 is usually used to monitor the neurite outgrowth and provide a subtler indication of neuronal function (Figure 7B). From the results, hippocampus in the AD mice treated with PBS or D-D/siRNA had a deletion of MAP2 expression, while the healthy mice had more positive expression of MAP2.

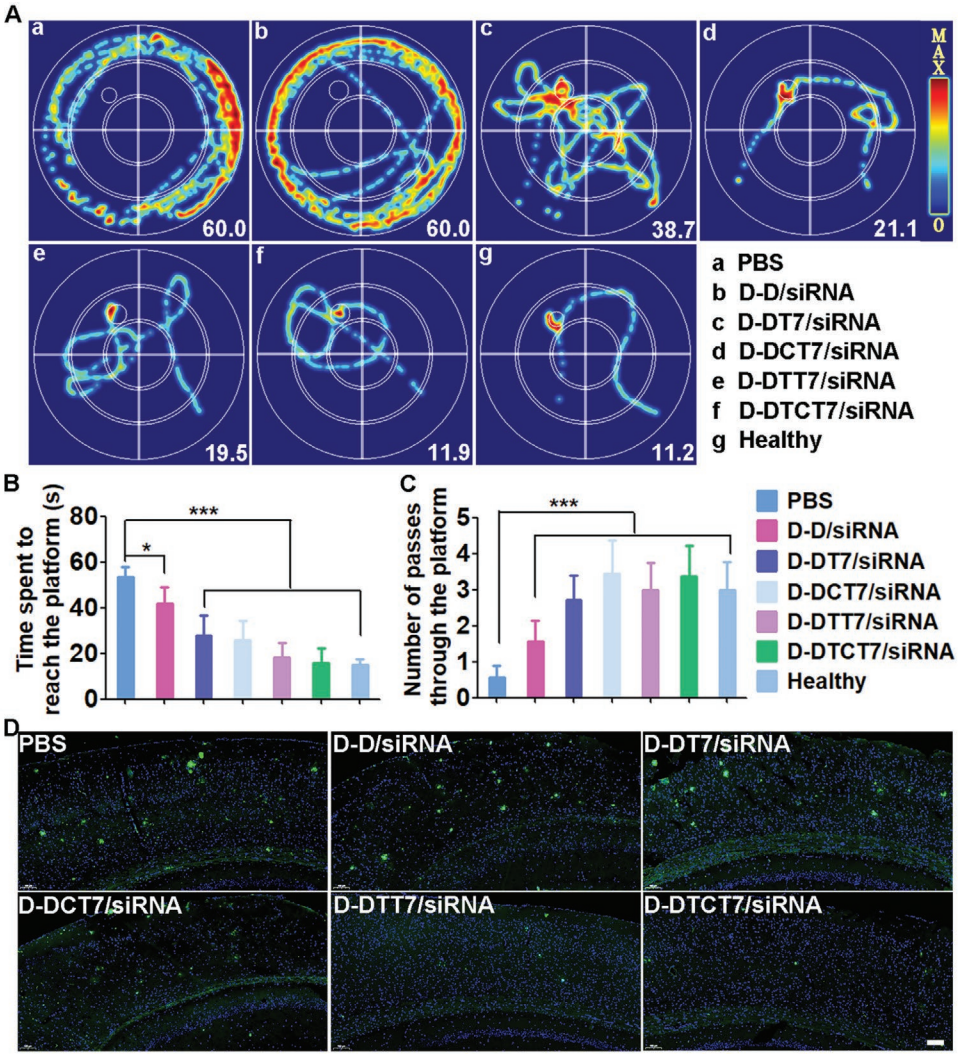

Figure 6. Learning acquisition and A$\beta_{1\text{-}42}$ plaques reduction. A) The representative swimming paths of mice in Morris water maze test, numbers in the lower right indicate the time spent to reach the platform. B) The time for mice to reach the platform in Morris water maze test. Data were presented as mean ± s.d. ($n = 9$). C) The frequency for the mice passing through the platform in the spatial probe test. Data were presented as mean ± SD ($n = 9$). D) Representative images of amyloid plaques stained by immunofluorescence in cortex region from APP/PS1 transgenic mice. Green represents A$\beta_{1\text{-}42}$ -stained plaques, blue represents nuclei stained by DAPI, and scale bar represents 100 µm.

After treatment with D-DCT7/siRNA, D-DTT7/siRNA, or D-DTCT7/siRNA, the positive rate of MAP2 was 6.8, 5.8, and 11.5 times higher than that in the PBS group, respectively (Figure 7C). Among them, the MAP2 expression in cleavage T7 group (D-DTCT7/siRNA) was most obvious. Accordingly, D-DTCT7/siRNA could not only effectively protect the neurons, but also increase the number of neurons to ameliorate the memory decline.

2.10. Gene Silencing Effects In Vivo

Next, we verified whether the enhanced memory and learning ability of the mice in the D-DTCT7/siRNA group was associated with the reduced expression of the target gene BACE1. BACE1 mRNA levels in the hippocampus were quantitatively measured by RT-PCR (Figure 7D). Compared with the healthy mice, the mRNA level of BACE1 in AD mice increased significantly. Among them, D-DCT7/siRNA (99.8% ± 10.9%) and D-DTCT7/siRNA (111.4% ± 18.5%) treatments significantly decreased BACE1 mRNA compared with PBS group (123.3% ± 45.9%), revealing cleavable T7 modified nanoparticles could effectively reach the target sites and inhibit the expression of BACE1 to obtain a better therapeutic effect.

2.11. Evaluation of Systemic Toxicity

The in vivo toxicity of the nanoparticles was evaluated by body weight changes, organ H&E staining, and biochemical indicators. First, adult healthy mice were treated with different formulations and their body weights were recorded every 3 days). There was no obvious difference in the body weights among all the groups (Figure S13B, Supporting Information). After

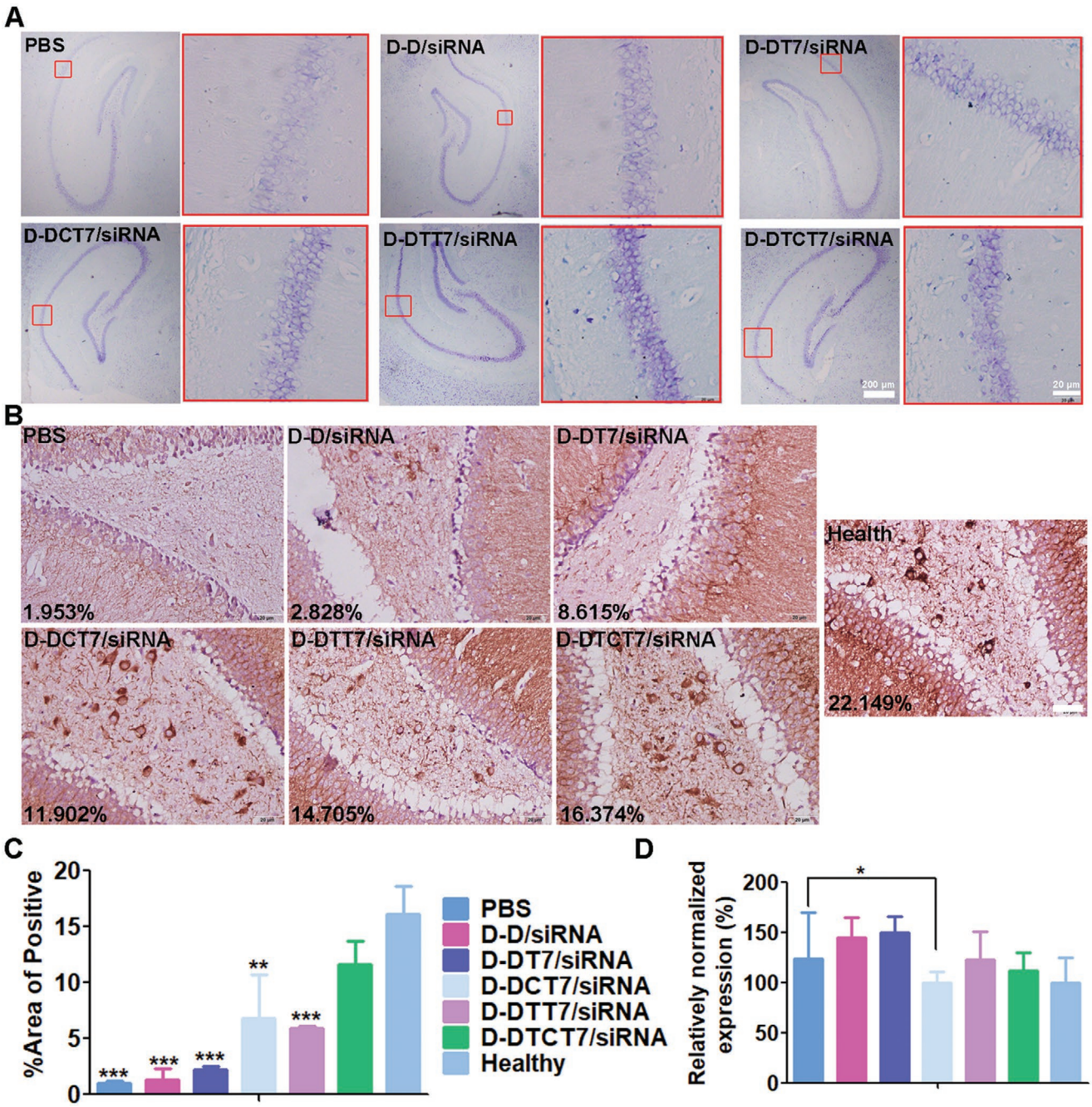

Figure 7. Neuroprotective and gene silencing effects in vivo. A) Nissl staining in the hippocampus of mice in different treatment groups. The red box shows the hippocampal CA1 area. Scale bars represent 200 and 20 μm, respectively. B) Immunohistochemical of neuron skeleton protein MAP2, brown represents the positive area. The lower left digits represent the positive rate of MAP2 expression. Scale bars represent 20 μm. C) Quantification of the positive rate of MAP2 ($n = 3$). D) Quantitative expression of BACE1 mRNA in the hippocampus of mice in different treatment groups. Data were presented as mean ± SD ($n = 3$).

2 weeks, the mice were sacrificed and their blood samples were prepared. Blood biochemical indexes showed that ALT and AST in the treatment groups increased slightly compared with the PBS group, but there was no significant change in the other indexes (Tables S2–S4, Supporting Information). Besides, H&E staining showed that there was no visible pathological change of organs in each group (Figure S13C, Supporting Information). Therefore, this dual-targeting siRNA/drug delivery depot possessed potential for clinical application due to its in vivo safety.

3. Conclusion

In summary, we designed an endo/lysosome-escapable D-DTCT7/siRNA delivery depot, which could programmatically

target BBB and neurons for improving the treatment of Alzheimer's disease. First, cellular uptake validated that D-DTCT7/siRNA could specifically recognize the TfR on the BBB endothelial cells and increase the internalization through the receptor-mediated endocytosis pathway. Second, subcellular localization, in vitro BBB model transcytosis and in vivo fluorescence imaging investigation demonstrated that the acid-responsive linker between T7 peptides and nanoparticles could be cleaved in the endo/lysosome, so that the nanoparticles quickly escaped from endo/lysosome and then targeted to neurons in the brain parenchyma through Tet1 peptide guiding. Finally, water maze test and immunohistochemistry displayed that the nanoparticles released the BACE1 siRNA/Dp to inhibit the production of Aβ in the cerebral cortex, and to restrain the p-Tau-associated fiber tangles in neurons. As a result, D-DTCT7/siRNA treatment significantly improved the learning acquisition and mitigated the neurological damage of AD mice. Furthermore, such a BBB and neuron-targeted drug delivery approach could be adopted to enhance the therapeutic efficacy for other brain diseases.

4. Experimental Section

Materials, Cells, and Animals: DGL generation 3 was purchased from Colcom (France). The negative control siRNA (sense: UUCUCCGAACGUGUCACGUTT, antisense: ACGUGACACGUUCGGAGAATT), BACE1 siRNA (sense: GCUUUGUGGAGAUGGUGGATT, antisense: UCCACCAUCUCCACAAAGCTT), and FAM-labeled siRNA were obtained from Sangon Biotech (Shanghai, China). Dp (*d*-TLKIVWGKKKC), Tet1 (HLNILSTLWKYR), and T7 (HAIYPRH) were synthesized by Phtdpeptides Co., Ltd. (Zhengzhou, China). Aβ_{1-42} was purchased from GL Biochem Ltd. (Shanghai, China). Bis-*N*-hydroxylsuccinimide (NHS) functionalized polyethylene glycol (NHS-PEG-NHS) was purchased from Nanocs Inc. (USA). Maleimide-poly (Ethylene Glycol)-Succinimidyl Valerate (Mal-PEG-SVA) was purchased from Laysan Bio Inc. (USA). RNase A was purchased from Solarbio Life Sciences (Beijing, China). LysoTracker Red DND-99 was purchased from Molecular Probes, Invitrogen (USA). The MAP2 antibody was purchased from Abclonal (China). Anti-beta Amyloid 1–42 antibody was purchased from Abcam (UK). Thioflavin-T was purchased from Sigma-Aldrich Co. LLC (USA). The bEnd.3 and PC12 cell lines were obtained from the Chinese Academy of Sciences Cell Bank (Shanghai, China). Dulbecco's Modified Eagle's Medium (DMEM), trypsin-EDTA solutions, and FBS were purchased from Gibco (USA). All of the other chemicals were analytical or reagent grade.

The nude mice were purchased from Byrness Weil Biotech. Ltd. (Chongqing, China). Kunming mice were obtained from Chengdu Dashuo Lab. Animal Co., Ltd. (Chengdu, China). B6C3-Tg (APPswePSEN1DE9)/Nju mice were purchased from the Nanjing Biomedical Research Institute of Nanjing University (Nanjing, China). All animals were maintained under standard housing conditions. All animal studies were performed under the guidelines evaluated and approved by the ethics committee of Sichuan Provincial People's Hospital and that of Sichuan University.

Gel Retardation Assay: 2% agarose was dissolved in Tris-borate-EDTA (TBE) buffer to form agarose gel. D-DTCT7/siRNA was prepared at different N/P ratios: 1, 2, 5, 10, 20, and 40, respectively. After being mixed with loading buffer, nanoparticles were loaded in gel and worked voltage of 100 V on 20 min. The location of siRNA in the gel was analyzed and photographed on a UV illuminator.

Quantified Fluorescence Intensity by Flow Cytometry: bEnd.3 and PC12 cells were seeded at a density of 1×10^4 cells per well in 12-well plates and cultured at 37 °C for 24 h. The FITC-labeled nanoparticles (40 μg mL^{-1} DGL with 7 μg mL^{-1} siRNA) were then incubated with the cells for 1, 2, and 4 h at 37 °C, the cells were washed three times with PBS. The single-cell suspension was prepared and quantified by flow cytometry (BD FACS Celesta, USA).

Cells Imaging: The same cells were seeded in the 6-well plate at a density of 5×10^5 cells per well cultured at 37 °C for 24 h. The FITC-loaded nanoparticles were then incubated with the cells for 2 h, followed by staining with 50 nM LysoTracker Red DND-99 for 30 min and 5 μg mL^{-1} DAPI for 5 min. Co-localization was observed with laser scanning confocal microscopy (Eclipse Ti, Nikon, Japan).

In Vitro BBB Model Transcytosis: The nanoparticles (prepared using FAM-labeled siRNA) were put into bEnd.3 monolayer coated transwells.[34,44] After 20, 40 min, 1, 2, 4, 6, 8, and 12 h, the fluorescence intensity of liquid in the lower chamber was measured separately by a Fluorescence Spectrophotometer (Labsolutiongs RF, Shimadzu, Japan). After 12 h, the bEnd.3 monolayers on the plates were processed and imaged by a confocal microscope.

Quantitative Real-Time PCR: In vitro knockdown efficiency was measured by qRT-PCR (Bio-red CFX96). PC12 cells were seeded at a density of 2×10^4 cells mL^{-1} in 6-well plates as above. After 24 h treatment with D-DT/siRNA and D-DTT7/siRNA (40 μg mL^{-1} DGL with 7 μg mL^{-1} siRNA), total RNA was extracted using the Cell Total RNA Isolation Kit (Foregene, China). qRT-PCR was performed by Real-Time PCR Easy -SYBR Green I (Foregene, China) using the following primers: BACE1: F, gctgcagtcaagtccatcaa; R, attgctgaggaaggatggtg; and β-actin: F, ccacaccccgccagttc; R, gacccatacccaccatcacacc.

In Vivo Imaging: The AD mice were intravenously injected at a dose of 5 mg kg^{-1} DGL (879 μg kg^{-1} siRNA) with the Cy5.5-labeled nanoparticles (D-D/siRNA, D-DT/siRNA, D-DT7 siRNA, D-DCT7/siRNA, D-DTT7/siRNA, and D-DTCT7/siRNA). After injection 2, 4, 8, 12, 24, 32, and 48 h, the mice were imaged using the Lumina III Imaging System (PerkinElmer, USA). At 48 h, the mice were sacrificed, and their tissues and brains were separated. The images were captured as above. The organs and brains were soaked into 4% paraformaldehyde for 24 h, dehydrated in sucrose solution, and embedded in Tissue-Tek O.C.T compound (Sakura Finetek, USA). Then all organs were sectioned at 10 μm with the freezing microtome (Leica CM1950, Germany). The other organs were stained with DAPI. The images were observed using a confocal microscope.

Immunohistochemistry After Treatment: 8-month-old double transgenic mice were divided into six groups on average ($n = 5$). The healthy control group was wild-type B6C3 mice. Nanoparticles (D-D/siRNA, D-DT7/siRNA, D-DCT7/siRNA, D-DTT7/siRNA, D-DTCT7/siRNA), and PBS were administered intravenously every other day at a dose of 2.5 mg kg^{-1} DGL (440 μg kg^{-1} siRNA). After 2 weeks of the administration, mice were sacrificed and their heart, liver, spleen, lung, kidney, and brain were sampled for H&E staining. In addition, the hippocampal slices were stained with Nissl. The immunohistochemical method was used to incubate antibody MAP2 to observe the positive rate of neuro synapses.

Immunofluorescence: After paraffin sections of brains were dewaxed with dibenzoyl, they were hydrated with 100%, 95%, 80%, 70% alcohol and pure water. After repairing the antigen with citric acid repair solution (pH 6.0), the sections were blocked and stained with primary Anti-Aβ_{1-42} antibody (dilution ratio 1:200). The slices were further stained with corresponding FITC-conjugated secondary antibodies (dilution ratio 1:500) at room temperature for 2 h. Tris-buffered saline was utilized for dilution and washing through all experimental procedures. Images were captured by a confocal microscope.

Morris Water Maze Test: The AD model mice were randomly divided into six groups ($n = 9$). Normal Kunming mice were used as healthy control. After 2 weeks of treatment as described above, spatial learning and memory ability of mice were evaluated by the Morris water maze test. The mice were put in a white round pool (100 cm in diameter and 50 cm in height), which contained a circular platform in the water. If the mice found the platform within 60 s, they would stay on the platform for 3 s for memory. If the mice did not find it, they would be guided to the platform for 3 s rest. The mice were trained for 5 days. After training, the platform was removed and the spatial probe test was carried out. They

were allowed to swim freely for 60 s. Average data from daily tests were used for statistical analysis. After the test, all mice were sacrificed and dissected. The brain (100 mg) was homogenized by a high-speed tissue grinder (Servicebio, Wuhan, China) to extract total protein and total RNA for qRT-PCR experiments.

Evaluation of Systemic Toxicity: Weighed once every 3 days of mice during the two weeks treatment. Besides, adult healthy mice were treated with the same dose of different nanoparticles (D-DCT7/siRNA, D-DTCT7/siRNA) and the blood samples were taken from all mice after 3 weeks. Then, blood biochemical indexes were detected. The cumulative toxicity of the nanoparticles was observed by H&E staining on the visceral slices of mice after treatment.

Statistical Analysis: The paired Student's *t*-test was used in the comparative analysis of each group. $p < 0.05$, $p < 0.01$, and $p < 0.001$ were considered a statistically significant difference and remarked with *, **, and ***, respectively.

Supporting Information

Supporting Information is available from the Wiley Online Library or from the author.

Acknowledgements

L.C. and C.Y. contributed equally to this work. The authors gratefully acknowledge the financial support from National Natural Science Foundation of China (81872806, 81961138009, 81972901), Research Funds of Sichuan Science and Technology Department (19YYJC2250, 2019YFS0514), 111 Project (B18035), and the Fundamental Research Funds for the Central Universities. The authors are grateful to Dr. Chenghui Li (Analytical & Testing Center, Sichuan University) for her technical help.

Conflict of Interest

The authors declare no conflict of interest.

Keywords

acid-responsive, Alzheimer's disease, blood–brain barrier transcytosis, neuron targeted

Received: November 30, 2019
Revised: March 22, 2020
Published online:

[1] D. J. Selkoe, J. Hardy, *EMBO Mol. Med.* **2016**, *8*, 595.
[2] M. Tajes, E. Ramos Fernández, X. Weng Jiang, M. Bosch Morató, B. Guivernau, A. Eraso Pichot, B. Salvador, X. Fernàndez Busquets, J. Roquer, F. J. J. Muñoz, *Mol. Membr. Biol.* **2014**, *31*, 152.
[3] C. Li, J. Wang, Y. Wang, H. Gao, G. Wei, Y. Huang, H. Yu, Y. Gan, Y. Wang, L. Mei, H. Chen, H. Hu, Z. Zhang, Y. Jin, *Acta Pharm. Sin. B* **2019**, *9*, 1145.
[4] W. A. Banks, *Nat. Rev. Drug Discovery* **2016**, *15*, 275.
[5] C. E. G. Leyns, M. Gratuze, S. Narasimhan, N. Jain, L. J. Koscal, H. Jiang, M. Manis, M. Colonna, V. M. Y. Lee, J. D. Ulrich, D. M. Holtzman, *Nat. Neurosci.* **2019**, *22*, 1217.
[6] W. Jagust, *Nat. Rev. Neurosci.* **2018**, *19*, 687.
[7] M. Nair, R. D. Jayant, A. Kaushik, V. Sagar, *Adv. Drug Delivery Rev.* **2016**, *103*, 202.
[8] H. Gao, *Acta Pharm. Sin. B* **2016**, *6*, 268.
[9] G. Huile, P. Shuaiqi, Y. Zhi, C. Shijie, C. Chen, J. Xinguo, S. Shun, P. Zhiqing, H. Yu, *Biomaterials* **2011**, *32*, 8669.
[10] H. Gao, *J. Neuroimmune Pharmacol.* **2017**, *12*, 6.
[11] C. Hu, X. Yang, R. Liu, S. Ruan, Y. Zhou, W. Xiao, W. Yu, C. Yang, H. Gao, *ACS Appl. Mater. Interfaces* **2018**, *10*, 22571.
[12] S. Ruan, M. Yuan, L. Zhang, G. Hu, J. Chen, X. Cun, Q. Zhang, Y. Yang, Q. He, H. Gao, *Biomaterials* **2015**, *37*, 425.
[13] S. Ruan, W. Xiao, C. Hu, H. Zhang, J. Rao, S. Wang, X. Wang, Q. He, H. Gao, *ACS Appl. Mater. Interfaces* **2017**, *9*, 20348.
[14] D. T. Wiley, P. Webster, A. Gale, M. E. Davis, *Proc. Natl. Acad. Sci. U. S. A.* **2013**, *110*, 8662.
[15] S. Ruan, L. Qin, W. Xiao, C. Hu, Y. Zhou, R. Wang, X. Sun, W. Yu, Q. He, H. Gao, *Adv. Funct. Mater.* **2018**, *28*, 1802227.
[16] P. Zhang, L. Hu, Q. Yin, Z. Zhang, L. Feng, Y. Li, *J. Controlled Release* **2012**, *159*, 429.
[17] J. H. Lee, J. A. Engler, J. F. Collawn, B. A. Moore, *Eur. J. Biochem.* **2001**, *268*, 2004.
[18] S. Oh, B. J. Kim, N. P. Singh, H. Lai, T. Sasaki, *Cancer Lett.* **2009**, *274*, 33.
[19] J. K. Liu, Q. Teng, M. Garrity-Moses, T. Federici, D. Tanase, M. J. Imperiale, N. M. Boulis, *Neurobiol. Dis.* **2005**, *19*, 407.
[20] S. A. Townsend, G. D. Evrony, F. X. Gu, M. P. Schulz, R. H. Brown, R. Langer, *Biomaterials* **2007**, *28*, 5176.
[21] P. Wang, X. Zheng, Q. Guo, P. Yang, X. Pang, K. Qian, W. Lu, Q. Zhang, X. Jiang, *J. Controlled Release* **2018**, *279*, 220.
[22] I. Benilova, E. Karran, B. De Strooper, *Nat. Neurosci.* **2012**, *15*, 349.
[23] C. R. Jack Jr., H. J. Wiste, T. M. Therneau, S. D. Weigand, D. S. Knopman, M. M. Mielke, V. J. Lowe, P. Vemuri, M. M. Machulda, C. G. Schwarz, J. L. Gunter, M. L. Senjem, J. Graff-Radford, D. T. Jones, R. O. Roberts, W. A. Rocca, R. C. Petersen, *J. Am. Med. Assoc.* **2019**, *321*, 2316.
[24] J. M. Long, D. M. Holtzman, *Cell* **2019**, *179*, 312.
[25] L. M. Ittner, J. Gotz, *Nat. Rev. Neurosci.* **2011**, *12*, 67.
[26] C. Li, J. Gotz, *Nat. Rev. Drug Discovery* **2017**, *16*, 863.
[27] Z. He, J. L. Guo, J. D. McBride, S. Narasimhan, H. Kim, L. Changolkar, B. Zhang, R. J. Gathagan, C. Yue, C. Dengler, A. Stieber, M. Nitla, D. A. Coulter, T. Abel, K. R. Brunden, J. Q. Trojanowski, V. M. Lee, *Nat. Med.* **2018**, *24*, 29.
[28] E. B. Lee, B. Zhang, K. Liu, E. A. Greenbaum, R. W. Doms, J. Q. Trojanowski, V. M. Y. Lee, *J. Cell Biol.* **2005**, *168*, 291.
[29] Y. Jiang, K. A. Mullaney, C. M. Peterhoff, S. Che, S. D. Schmidt, A. Boyer-Boiteau, S. D. Ginsberg, A. M. Cataldo, P. M. Mathews, R. A. Nixon, *Proc. Natl. Acad. Sci. U. S. A.* **2010**, *107*, 1630.
[30] I. Hussain, J. Hawkins, D. Harrison, C. Hille, G. Wayne, L. Cutler, T. Buck, D. Walter, E. Demont, C. Howes, A. Naylor, P. Jeffrey, M. I. Gonzalez, C. Dingwall, A. Michel, S. Redshaw, J. B. Davis, *J. Neurochem.* **2007**, *100*, 802.
[31] O. Singer, R. A. Marr, E. Rockenstein, L. Crews, N. G. Coufal, F. H. Gage, I. M. Verma, E. Masliah, *Nat. Neurosci.* **2005**, *8*, 1343.
[32] T. E. Park, B. Singh, H. Li, J. Y. Lee, S. K. Kang, Y. J. Choi, C. S. Cho, *Biomaterials* **2015**, *38*, 61.
[33] X. Zheng, X. Pang, P. Yang, X. Wan, Y. Wei, Q. Guo, Q. Zhang, X. Jiang, *Acta Biomater.* **2017**, *49*, 388.
[34] Q. Guo, X. Zheng, P. Yang, X. Pang, K. Qian, P. Wang, S. Xu, D. Sheng, L. Wang, J. Cao, W. Lu, Q. Zhang, X. Jiang, *Acta Pharm. Sin. B* **2019**, *9*, 590.
[35] S. A. Sievers, J. Karanicolas, H. W. Chang, A. Zhao, L. Jiang, O. Zirafi, J. T. Stevens, J. Münch, D. Baker, D. Eisenberg, *Nature* **2011**, *475*, 96.
[36] Y. Liu, S. An, J. Li, Y. Kuang, X. He, Y. Guo, H. Ma, Y. Zhang, B. Ji, C. Jiang, *Biomaterials* **2016**, *80*, 33.
[37] R. Huang, S. Liu, K. Shao, L. Han, W. Ke, Y. Liu, J. Li, S. Huang, C. Jiang, *Nanotechnology* **2010**, *21*, 265101.

[38] A. Mokhtarzadeh, A. Alibakhshi, M. Hashemi, M. Hejazi, V. Hosseini, M. de la Guardia, M. Ramezani, *J. Controlled Release* **2017**, *245*, 116.
[39] R. Liu, M. Yu, X. Yang, C. S. Umeshappa, C. Hu, W. Yu, L. Qin, Y. Huang, H. Gao, *Adv. Funct. Mater.* **2019**, *29*, 1808462.
[40] R. Liu, W. Xiao, C. Hu, R. Xie, H. Gao, *J. Controlled Release* **2018**, *278*, 127.
[41] L. Wang, D. Wu, H. Xu, Y. You, *Angew. Chem., Int. Ed.* **2016**, *55*, 755.
[42] N. S. Gandhi, R. K. Tekade, M. B. Chougule, *J. Controlled Release* **2014**, *194*, 238.
[43] J. A. Brown, V. Pensabene, D. A. Markov, V. Allwardt, M. D. Neely, M. Shi, C. M. Britt, O. S. Hoilett, Q. Yang, B. M. Brewer, P. C. Samson, L. J. McCawley, J. M. May, D. J. Webb, D. Li, A. B. Bowman, R. S. Reiserer, J. P. Wikswo, *Biomicrofluidics* **2015**, *9*, 054124.
[44] M. Yu, D. Su, Y. Yang, L. Qin, C. Hu, R. Liu, Y. Zhou, C. Yang, X. Yang, G. Wang, H. Gao, *ACS Appl. Mater. Interfaces* **2019**, *11*, 176.
[45] R. Yan, R. Vassar, *Lancet Neurol.* **2014**, *13*, 319.
[46] V. Szegedi, G. Juhasz, E. Rozsa, G. Juhasz-Vedres, Z. Datki, L. Fulop, Z. Bozso, A. Lakatos, I. Laczko, T. Farkas, Z. Kis, G. Toth, K. Soos, M. Zarandi, D. Budai, J. Toldi, B. Penke, *FASEB J.* **2006**, *20*, 1191.